Journal of Alloys and Compounds, *177* (1991) 229–244
JAL 0074

Difference between mechanical alloying and mechanical disordering in the amorphization reaction of $Al_{50}Ta_{50}$ in a rod mill

M. Sherif El-Eskandarany, Kiyoshi Aoki and Kenji Suzuki
Institute for Materials Research, Tohoku University, Sendai 980 (Japan)

(Received May 28, 1991; in final form July 3, 1991)

Abstract

Amorphous $Al_{50}Ta_{50}$ alloy powders have been synthesized by mechanical alloying (MA) from elemental powders of aluminium and tantalum, and mechanical disordering (MD) from crystalline intermetallic compound powders of AlTa respectively using the rod milling technique. The mechanically alloyed and the mechanically disordered alloy powders were characterized by X-ray diffraction, scanning electron microscopy, electron probe microanalysis, transmission electron microscopy, differential thermal analysis, differential scanning calorimetry and chemical analysis. The results have shown that the crystal-to-amorphous transformation in the MD process occurs through one stage, while the crystalline-to-amorphous formation in the MA process occurs through three stages. At the early and intermediate stages of the MA time, heating the alloy powders to 700 K leads to the formation of an amorphous phase by a solid-state amorphizing reaction. At the final stage of the MA time, the amorphous phase is crystallized through a single sharp exothermic peak. Contrary to this, amorphous alloy powders produced by MD are crystallized through two broad exothermic peaks.

1. Introduction

The solid-state amorphizing reaction has received great attention since it was investigated by Schwarz and Johnson in 1983 [1]. A special type of solid-state reaction, which is called ball-milling, was discovered by Koch *et al.* [2] for producing amorphous alloy powders from pure nickel and niobium powders. So far, ball-milling has been used successfully for preparing many amorphous alloy powders [3–5] and metal nitrides [6] at room temperature.

In 1990, El-Eskandarany *et al.* [7] reported another novel technique for producing amorphous $Al_{30}Ta_{70}$ alloy powders from pure aluminium and tantalum powders by rod-milling. The rod-milling technique has been accepted as a successful method for producing amorphous alloy powders with low degree of contamination through solid-state amorphizing reaction.

In fact, there are only two categories of amorphization by ball-milling and/or rod-milling, that is to say, mechanical alloying (MA) and mechanical grinding (MG). The terms mechanical grinding [8] or mechanical milling [9] are usually used to express the crystal-to-amorphous transformation without compositional change. In this study, we shall use mechanical disordering

0925-8388/91/$3.50

(MD) as a more suitable terminology which reflects the mechanism of crystal-to-amorphous transformation in much better understanding. The MA process synthesizes amorphous alloy powders by reacting elemental crystalline powders and/or powders of the intermetallic compounds, being accompanied with a negative heat of formation [10]. However, in the MD process the crystalline alloy or compound powders are transformed into the amorphous solid state by relaxing the short-range order without compositional changes [11]. The MA and MD processes are reactions going in thermodynamically opposite directions.

Recently, phase relationship have been investigated in the Al–Ta system [12]. The Al–Ta equilibrium diagram is composed of four intermediate phases: $AlTa_2$, AlTa, Al_2Ta and Al_3Ta. In this study, the equiatomic compound of AlTa was chosen as a starting material for both MA and MD methods. The aim of this study is to investigate the main difference(s) between the two processes for producing $Al_{50}Ta_{50}$ amorphous alloy powders. The results will be discussed from the point of view of structure, morphology and calorimetry. Moreover, we attempt to establish clear answers to the questions of how, what and why the amorphization via MA and MD are different.

2. Experimental Procedure

In this study both MA and MD processes were used to produce amorphous $Al_{50}Ta_{50}$ alloy powders. For the MA process, elemental powders of aluminium (-325 mesh, 99.999%) and tantalum (-150 mesh, 99.99%) were mixed in a glove box under a purified argon gas atmosphere to give the desired average composition. Whereas, the starting material for the MD process was prepared by arc-melting nominal amounts of 99.999% pure aluminium and 99.999% pure tantalum in an argon gas atmosphere (O_2 less than 0.2 p.p.m.), purified with a titanium getter. The ingot was remelted five times, reweighed and checked metallographically. After the ingot had been crushed to powders using a stainless steel (SUS 304) mortar and pestle, the powders were classified in diameter to less than 50 μm using screen analysis and then analyzed using the ICP emission method. The MA and MD processes were performed by the rod milling (RM) technique. The RM technique used in this study is essentially the same as that described in a previous paper [7].

The MA and MD experiments were stopped at regular intervals (starting after 3.6 ks) and a small amount of the rod-milled alloy powders was taken out from the vial in a glove box filled with high-purity argon gas. The progress of amorphization for MA and MD alloy powders was followed by X-ray diffraction (XRD) with Mo Kα, differential thermal analysis (DTA) under an argon atmosphere at a heating rate of 0.33 K s^{-1} and differential scanning calorimetry (DSC) in a flow of argon (0.83 ml s^{-1}). The morphology of the alloy powders was studied by scanning electron microscopy (SEM), electron probe microanalysis (EPMA) and transmission electron microscopy (TEM) using a 200 kV microscope. The samples for TEM observations were prepared

by mounting the powders on a copper microgrid. Moreover, the ICP emission method was used to analyze the contents of aluminium and tantalum, and the degree of iron contamination in the milled powders. Details of these measurements have been described in a previous paper [13].

3. Results

3.1. X-ray diffraction

The XRD patterns of mechanically alloyed and disordered $Al_{50}Ta_{50}$ are shown as a function of the rod-milling time in Figs. 1(a) and 1(b) respectively. As shown in Fig. 1(a), the intensities of the Bragg peaks for pure aluminium and tantalum powders decrease simultaneously with increasing the MA time. At the intermediate stage of MA (720 ks) all of the minor Bragg peaks from elemental aluminium and tantalum crystals decrease with increasing MA time. After 86 ks of milling, the Bragg peaks from elemental f.c.c. Al (200), (220) and (311) reflections disappear. In addition, the intensities of the Bragg peaks from elemental b.c.c. tantalum decrease quickly. During the intermediate stage (360–720 ks) of MA time, the major Bragg peaks from pure Al (111) and Ta (110) and (211) reflections become wider, indicating the formation of an amorphous phase. Furthermore, the other Bragg peaks of pure aluminium and tantalum have almost disappeared. Towards the end of the MA time (1440 ks) a homogeneous amorphous phase is formed, characterized by broad and smooth peaks.

As presented in Fig. 1(b), the starting powder of AlTa intermetallic compound has an XRD pattern with sharp Bragg peaks. The intensities of

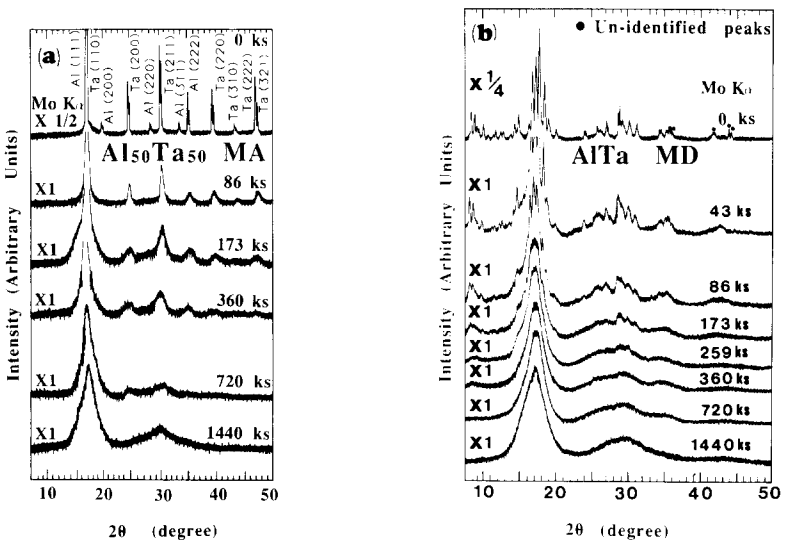

Fig. 1. XRD patterns of $Al_{50}Ta_{50}$ alloy powders as a function of (a) MA time and (b) MD time.

these peaks decrease with increasing MD time. A halo pattern with no sharp Bragg peaks was obtained after 360 ks of MD time. At the final stage of milling (1440 ks) a homogeneous phase was formed, because small angle scattering at 2θ less than 10° completely disappeared.

3.2. Morphology

Figure 2 shows scanning electron micrographs of the MA and MD $Al_{50}Ta_{50}$ powders after selected rod-milling times. The typical starting powders at 0 ks of MA and MD are shown in Figs. 2(a) and 2(b) respectively. At the starting stage, the MD particles are block-like whilst the MA particles have a flake-like morphology. After 22 ks of MA time, the powder particles tend to agglomerate in size extending to more than 300 μm in diameter, as shown in Fig. 2(c). In contrast, after 22 ks of MD the particles size is reduced to less than 20 μm in diameter and the shape of the starting materials has changed to a globe-like morphology, as illustrated in Fig. 2(d).

Figure 3 shows the change of particle size for MA and MD $Al_{50}Ta_{50}$ powders as a function of the rod-milling time. The size of the powders were determined from the SEM observations. The process for forming alloy powders differs for MA and MD. The milling process performed by the MA process can be classified into three stages [4, 14]. At the initial stage (4–22 ks), which is called the agglomeration stage, the starting elemental powders of aluminium and tantalum agglomerate during this early stage of milling to form powders of greater diameter, as large as several hundred μm to reach a peak of almost 300 μm after 22 ks of milling as shown in Fig. 2(c). During this stage of milling, the characteristic structure containing aluminium and tantalum layers appears, as shown in Fig. 4(a). Using an electron microscope analysis it was found that the gray parts are aluminium layers and the dark matrix is tantalum rich. In the middle stage, corresponding to the MA time from 22 to 360 ks, fragmentation with amorphizing reaction proceeds drastically by atomic diffusion through the interface between the layers. Moreover, the powder particles are subjected to continuous disintegration until the size of the powders is reduced to less than 10 μm in diameter, as shown in Figs. 2(e) and 3.

The MD process leads to a different behavior for the variation in powder diameters, as illustrated in Fig. 3. The starting powders of AlTa intermetallic compound are continuously reduced in size without any agglomerations or layer-structure morphology to form fine powders about 10 μm in diameter after only 22 ks, as shown in Fig. 2(f). Furthermore, in the MD, however, the size reduction of the particles proceeds at a high rate to provide a narrow size distribution, as shown in Fig. 3.

During the final stage of milling, which is called the homogenization stage (360–1440 ks) where the amorphous structure is homogenized, the particle size states of the MA and MD $Al_{50}Ta_{50}$ alloy powders is nearly the same, as shown in Fig. 3. Towards the end of the milling time (1440 ks), the shape and the size of both MA and MD amorphous $Al_{50}Ta_{50}$ alloy powders are almost the same, as shown in Figs. 2(g) and 2(h).

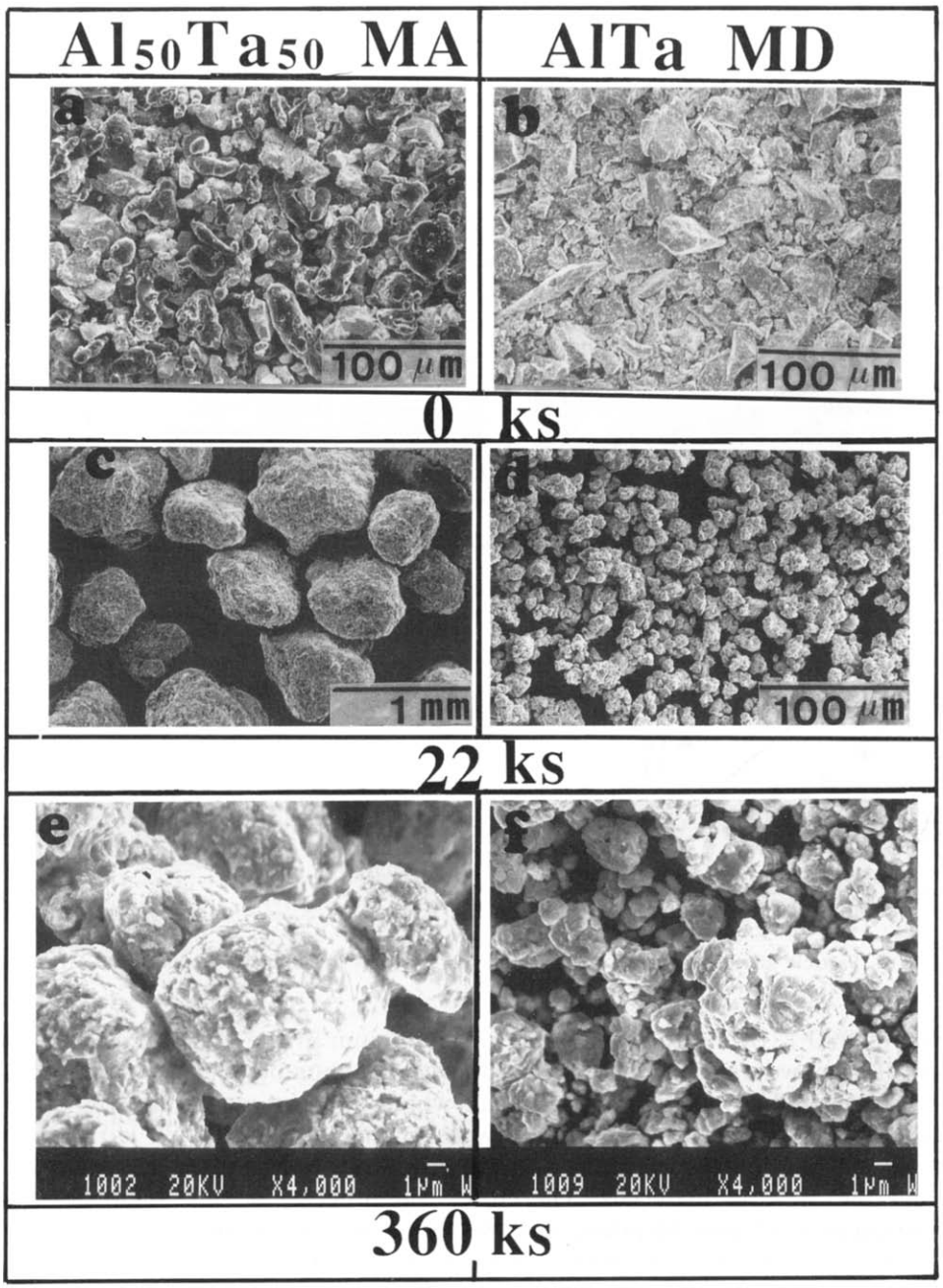

Fig. 2. Scanning electron micrographs of $Al_{50}Ta_{50}$ alloy powders as a function of MA and MD time.

3.3. Thermal analysis

Figure 5 shows the DTA curves for $Al_{50}Ta_{50}$ alloy powders as a function of the MA time. At 0 ks of milling, a sharp endothermic peak appears at

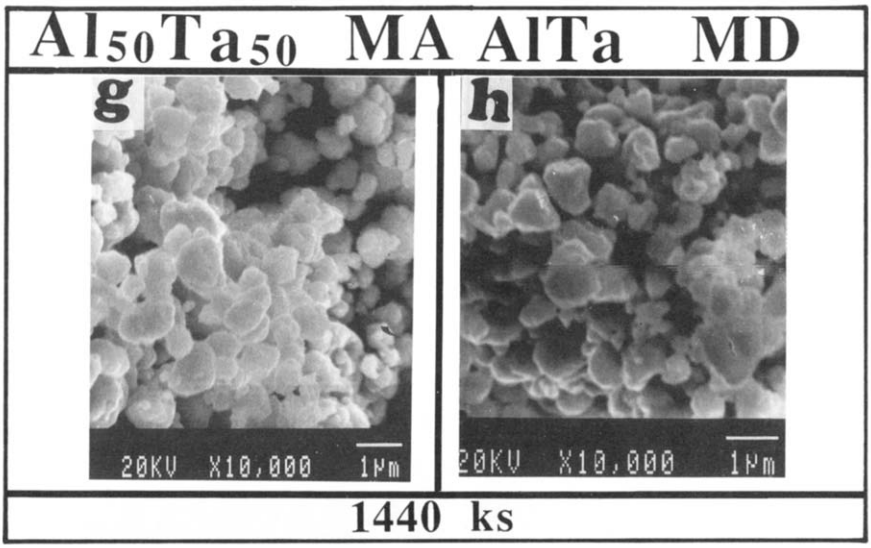

Fig. 2. (*continued*)

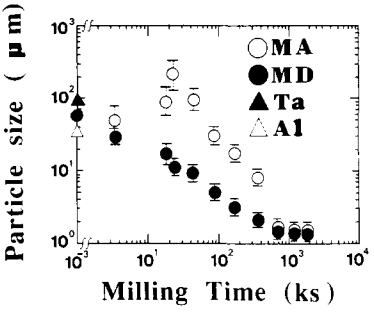

Fig. 3. Particle size distribution of $Al_{50}Ta_{50}$ alloy powders as a function of MA and MD time.

about 930 K owing to the melting of aluminium in the starting material of $Al_{50}Ta_{50}$ powders. The melt then reacts with tantalum powders in the mixture, characterized by an exothermic peak which appears at about 1190 K, as shown in Fig. 5. During the first few ks of the MA time (4–22 ks) there is no significant difference in the thermal properties between the alloy powders and the starting materials. Therefore, the process at this stage has the appearance of just blending the two elemental metal powders. Both the exothermic and the endothermic peaks disappear through the second heating runs, as illustrated by the dashed lines in Fig. 5. Contrary to this, a single broad exothermic peak appears at about 650 K and the exothermic reaction peak disappears after 43 ks of MA time. After 86 ks of milling, another broad exothermic peak appears above 800 K and the first exothermic peak becomes more sharper. This second exothermic peak is shifted to an elevated temperature and becomes sharp towards the end of the MA process (1440

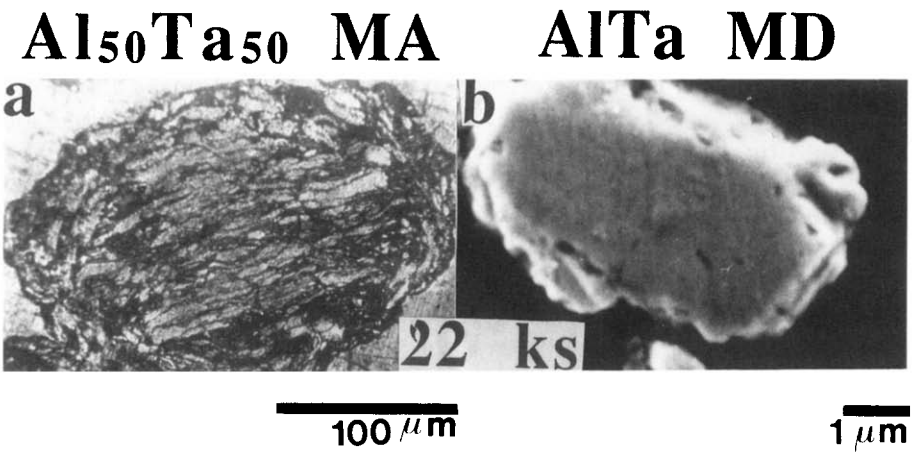

Fig. 4. Morphology of the powder particles as a function of MA and MD processes after 22 ks of milling: (a) optical micrographs of MA $Al_{50}Ta_{50}$ powders, (b) scanning electron micrographs of MD AlTa powders.

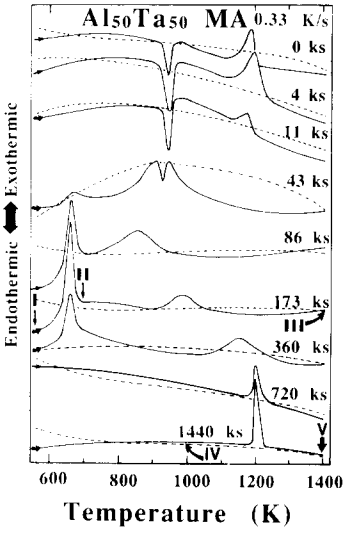

Fig. 5. DTA curves of $Al_{50}Ta_{50}$ alloy powders as a function of MA time.

ks). However, the temperature of the first exothermic peak, does not change with the milling time, as shown in Fig. 5.

In order to identify the origin of these exothermic reactions, three samples of 173 ks alloy powders were heated separately in the DTA for TEM investigations at I, II and III, as shown in Fig. 5. The TEM observations have allowed direct imaging of the phase formation for these samples. Figures

6(a) and 6(b) show TEM images that were obtained from sample I. The electron diffraction pattern from several regions of this sample show a ring–spot pattern that is characteristic of several simultaneously diffracting polycrystalline Al/Ta, as shown in Fig. 6(b). We should emphasize that no evidence for the formation of an amorphous phase could be observed. Contrary to this, the electron diffraction pattern of sample II taken at 700 K (Fig. 6(c)) indicates the formation of an amorphous phase, characterized by a clear visible halo pattern, as shown in Fig. 6(d). It is worth mentioning that almost 80% of the electron diffraction patterns for several regions of this sample showed the same pattern as that illustrated in Fig. 6(d). Whereas, only 20% of the diffraction patterns show the formation of an amorphous phase coexisting with Al/Ta polycrystals. Sample III taken at 1400 K (Fig. 6(e)) shows in all regions without any exceptions a ring–spot pattern as shown in Fig. 6(f). The ring pattern, which can be indexed as polycrystalline AlTa, is characteristic of crystallization of the amorphous phase. Furthermore, during the DTA measurements of MA $Al_{50}Ta_{50}$ after 1440 ks of milling time, two independent samples were taken far below the crystallization temperature, T_x, at 1000 K (IV), and well above T_x at 1400 K (V) for TEM observations, as shown in Fig. 5. The bright-field image for sample IV shows a fine structure with nanocrystalline dimensions, as presented in Fig. 7(a). The electron diffraction pattern for a selected area of this sample (Fig. 7(a) inset) shows a halo pattern indicating that the amorphous phase still exists at 1000 K. However, at 1400 K (sample V), the TEM image shows a microcrystalline structure, indicated by the grain growth morphology, as shown in Fig. 7(b). Moreover, the halo pattern is replaced with a spot–ring pattern which is indexed to the crystallization of the amorphous phase, as illustrated in Fig. 7(b).

The DSC curves for the low temperature range (500–800 K) of MA $Al_{50}Ta_{50}$ alloy powders are shown in Fig. 8 as a function of the milling time. DSC has been used to obtain the values of the amorphization temperature, T_a, and the enthalpy change of amorphization, ΔH_a, with greater accuracy. These values are plotted in Figs. 11 and 12 (above) as a function of the MA time.

However, in MD alloy powders the exothermic reaction peaks which are attributed to a solid-state amorphizing reaction at the fresh surfaces of Al/Ta boundaries, are absent, as shown in Fig. 9. The DTA curves of MD AlTa alloy powders reveal two exothermic peaks which developed during MD. After 1440 ks of MD time, a large exothermic peak is observed at about 1200 K and a smaller broad peak is detected at about 1330 K. To identify these two exothermic peaks, three samples were heated separately in the DTA. The first sample (I) was heated to 1000 K, well below the first peak, whilst the second sample (II) was heated to 1250 K, between the first and the second peaks, and the last sample (III) was taken after heating the sample to 1400 K, as shown in Fig. 9.

The role of temperature in determining the nucleation and growth morphology is shown by TEM micrographs in Fig. 10. At 1000 K (sample I)

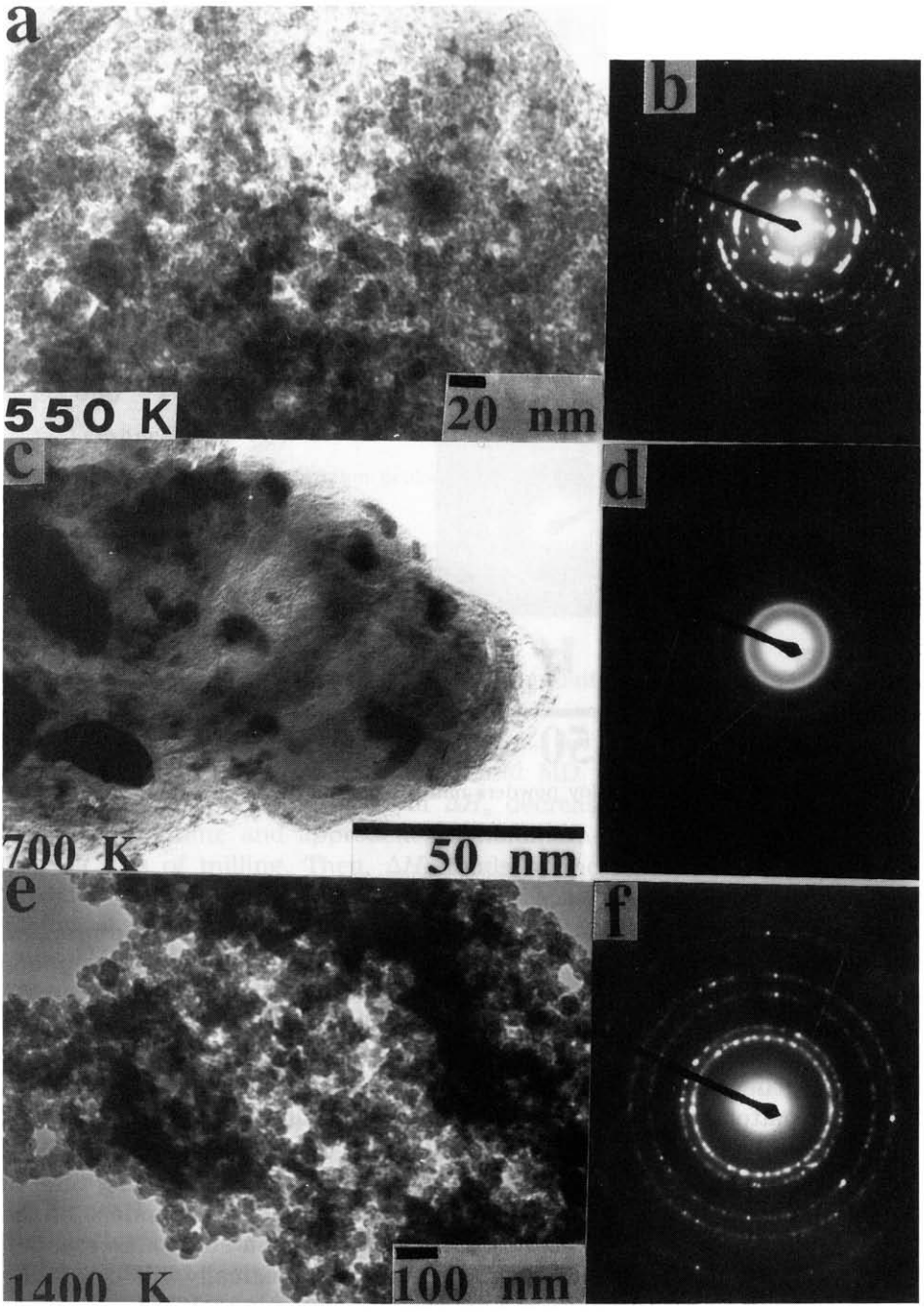

Fig. 6. The bright-field images and the corresponding diffraction patterns of $Al_{50}Ta_{50}$ alloy powders milled for 173 ks, then heated to (a) 550 K, (b) 700 K and (c) 1400 K.

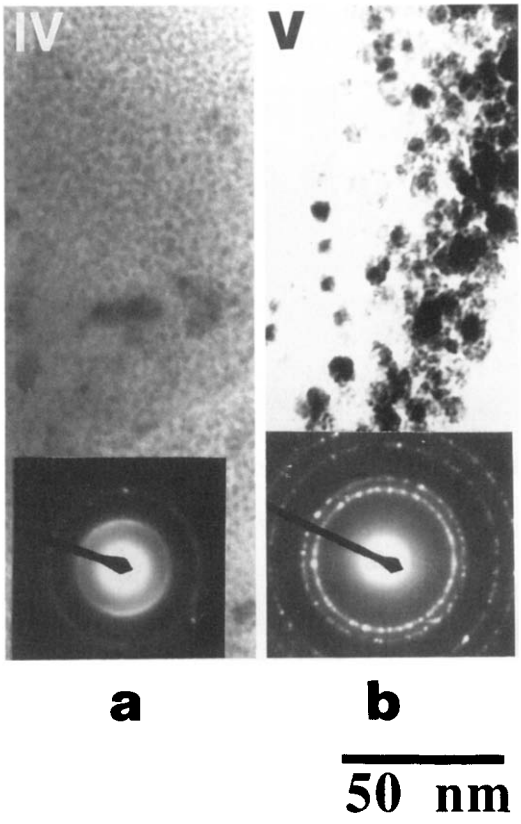

Fig. 7. TEM images of $Al_{50}Ta_{50}$ alloy powders milled for 1440 ks, then heated to (a) 1000 K and (b) 1400 K.

no microstructure of the size of 10 nm is observed and the halo-diffraction pattern from a selected area can indicate the existence of the amorphous phase, as illustrated in Fig. 10(a). However, in sample II, this halo-diffraction pattern coexists with polycrystalline AlTa as shown in Fig. 10(b). Moreover, the particles of sample II tend to grow in diameter. The particles of sample III tend to grow to a greater size, as shown in Fig. 10(c). Furthermore, the diffraction pattern shows a complete formation of the polycrystalline AlTa characterized by a spot–ring pattern, as illustrated by the inset of Fig. 10(c).

Figure 11 shows the correlation between T_a, T_x and the milling time of MA and MD. The value of T_a for MA alloy powders is independent of the milling time, which suggests that the amorphization by a solid-state reaction occurs simultaneously. Contrary to this, T_x increases drastically with increasing the MA time in the early and the intermediate stages of milling, indicating a continuous change of composition of the amorphous phase. T_x approaches a saturation value (1210 K) during the final stage of the MA time. In MD alloy powders, however, there is no big change in T_x, suggesting that the

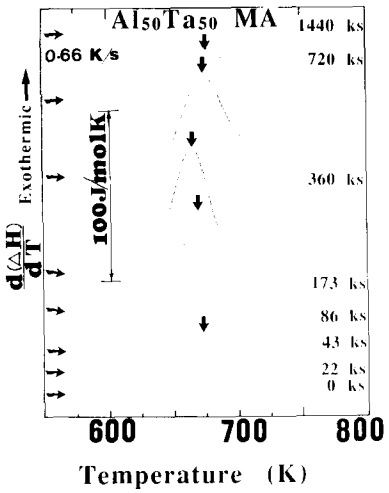

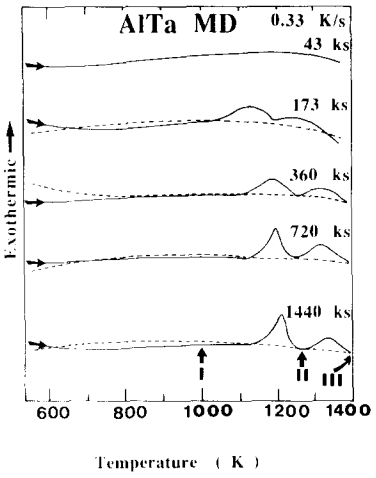

Fig. 8. DSC curves of amorphization peaks for $Al_{50}Ta_{50}$ alloy powders as a function of the MA time.

Fig. 9. DTA curves of $Al_{50}Ta_{50}$ alloy powders as a function of MD time.

process occurs homogeneously without compositional change, as illustrated in Fig. 11.

The enthalpy change of amorphization, ΔH_a, and crystallization, ΔH_x, as a function of MA (open symbols) and MD time (closed symbols) are presented in Fig. 12. The value of ΔH_a decreases sharply during the first ks of the MA time and approaches a minimum value of -4.37 kJ mol^{-1} after 173 ks of milling. Then, ΔH_a tends to increase monotonically to be zero after 900 ks of the MA time. ΔH_x of MA $Al_{50}Ta_{50}$ alloy powders was calculated from the area under the single crystallization exothermic peak, while ΔH_x for MD AlTa alloy powders was evaluated from the sum of the areas under the two crystallization exothermic peaks. The value of ΔH_x for MA $Al_{50}Ta_{50}$ alloy powders decreases monotonically with increasing rod-milling time and approaches a saturation value of about -40 kJ mol^{-1} after 1080 ks of milling. In MD AlTa ΔH_x approaches the same saturation value after only 720 ks of milling time.

3.4. Chemical analysis

Figure 13 shows the amount of iron contamination which usually comes from the milling tools as a function of MA and MD time. In the MA process, the iron content increases monotonically with increasing milling time and approaches a constant value of about 0.5 at.% after 720 ks of MA time. In the MD process, however, a drastic increase in iron content during the early and the intermediate stages of milling (0 to 360 ks) was observed. The iron contamination content reaches a constant value of about 1.0 at.%

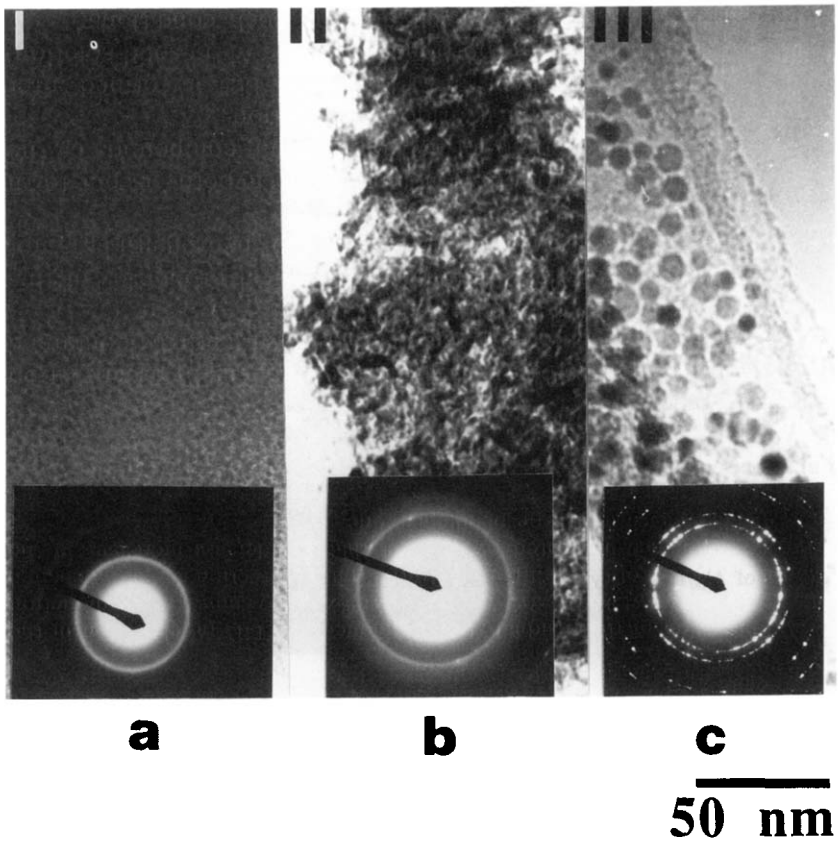

Fig. 10. TEM images of MD $Al_{50}Ta_{50}$ alloy powders milled for 1440 ks, then heated to (a) 1000 K, (b) 1250 K and (c) 1400 K.

4. Discussion

4.1. MA of elemental aluminium and tantalum powders

The MA process for producing $Al_{50}Ta_{50}$ alloy powders can be classified into three distinct stages, that is to say, agglomeration, amorphization and homogenization stages. The agglomeration stage (0–22 ks) may be defined as the stage in which the powder particles of aluminium and tantalum are agglomerated to a larger diameter, as was shown in Fig. 3. In this stage of milling, almost all of the starting material sticks to the surface of the rods. The particles that do not stick to the milling tools have a layered structure morphology, as shown in Fig. 4(a).

During the second stage of milling (22–360 ks), which is called the amorphization stage, a solid-state amorphizing reaction between the fresh

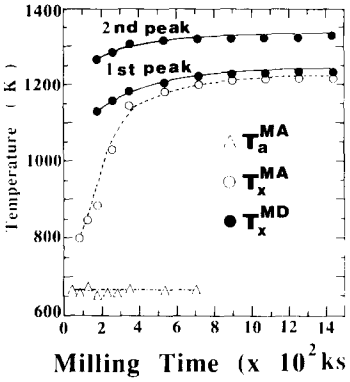

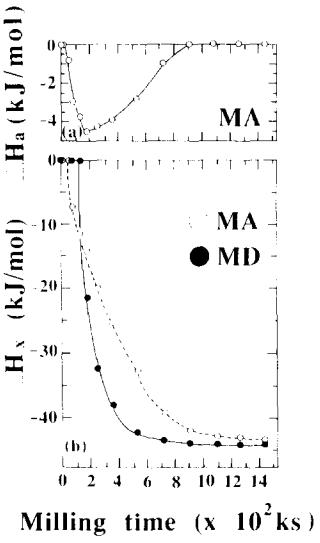

Fig. 11. Crystallization temperature, T_x, and amorphization temperature, T_a, of $Al_{50}Ta_{50}$ alloy powders as a function of milling time.

Fig. 12. Enthalpy change of $Al_{50}Ta_{50}$ as a function of MA and MD time: (a) amorphization enthalpy change, ΔH_a; (b) crystallization enthalpy change, ΔH_x.

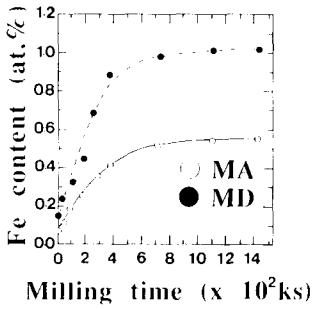

Fig. 13. Iron contamination content in $Al_{50}Ta_{50}$ alloy powders as a function of MA time and MD time.

surfaces of Al/Ta interfaces takes place. Furthermore, almost all of the particles contain many narrow layers in a good arrangement as a result of the shear force which was generated by the rods [14]. In this stage, two exothermic peaks have appeared during the DTA measurements, as shown in Fig. 5. The first exothermic peak occurs at a relatively low temperature (around 650 K), and the second one occurs at an elevated temperature. The TEM imaging as a powerful tool for investigating the origin of these peaks, has led us to attribute the first peak to solid-state amorphizing reaction between the fresh surfaces of aluminium and tantalum layers, whilst the second exothermic peak occurred due to the crystallization of the amorphous phase in the mechanically alloyed powders, as shown in Fig. 6. During this

stage, both T_x and $-\Delta H_x$ increase monotonically, suggesting a compositional change and an increase in the volume fraction of the amorphous alloy in the milled powders respectively.

The homogenization stage (720–1440 ks) refers to the last stage of milling in which a homogeneous amorphous phase was formed and has an XRD pattern with broad and smooth peaks. In this stage, the first exothermic peak had already disappeared, suggesting that the amorphization process was finished. Moreover T_x and ΔH_x have approached their saturation values, reflecting that the MA process occurs homogeneously. In addition, the layered-structure morphology as examined by cross-sectional SEM and EPMA of the particles, had already disappeared. The powder particles tend to appear in a spherical shape, as shown in Fig. 2(a).

4.2. MD of intermetallic compound AlTa powders

In fact, the MA and MD processes are similar in appearance, but differ completely in their mechanism. The MD process differs from the MA process in that the amorphization of a crystalline AlTa alloy requires an increase in its free energy from a lower level (more stable) to a higher level (less stable). By the rod-milling, the crystalline compound stores energy in the form of chemical disorder and point and lattice defects. The crystal-to-amorphous transformation requires a release of that stored energy to approach a specified value. In addition, the MD process is carried out through only one stage in which the powder particles are continuously disintegrated without agglomeration or formation of a layer-structure morphology of the particles. This is because the starting material here is an intermetallic compound itself, so that the solid-state amorphizing reaction cannot be considered in this case.

Moreover, the MD technique differs from the MA technique in the rate of amorphization. The amorphization process by MD occurs rapidly and much more homogeneously than that by MA. This is demonstrated by the nearly constant values of T_x and ΔH_x at the intermediate and final stages of milling (360–1440 ks).

Furthermore, the DTA curves of mechanically disordered AlTa alloy powders have shown that the exothermic peaks which is related to a solid-state amorphizing reaction are absent. However, the XRD patterns of the DTA sample for MD AlTa which was milled for 1440 ks and then annealed to 1400 K, did not show a clear difference in the Bragg peaks between them and those obtained in the case of the MA process. In addition, there is no significant difference in the Bragg peaks of as-cast AlTa crystalline compound and as-annealed MA and MD powders at 1440 K which were milled for 1440 ks. This may suggest that the amorphization by MA and MD leads to the formation of almost the same amorphous phase regardless of the great difference in the mechanism between the two processes. Furthermore, the two exothermic peaks which appear in the DTA curves of the 1440 ks alloy (see Fig. 9) show that the crystallization of MD alloy powders occurs in two stages. This may be attributed to nucleation and growth morphology of the heated alloy powders.

In addition, the iron contamination content in MD powders is higher than it is in MA powders, as was shown in Fig. 13. The higher iron contamination in MD powders can be attributed to the high hardness of the intermetallic compound powders used. In general, intermetallic compounds are harder than their constituent elements. Therefore, the high iron contamination seems to be a general disadvantage in the MD process.

5. Conclusions

In conclusion, for both mechanical alloying and mechanical disordering used in this study, the formation of $Al_{50}Ta_{50}$ amorphous alloy powders from elemental metal crystals of aluminium and tantalum and AlTa crystalline compound has been obtained. The differences between the two processes in the amorphization reaction of $Al_{50}Ta_{50}$ alloy powders are:

(1) The amorphization in the MA process takes place in three distinct stages, whereas in MD the amorphization occurs in only one stage.

(2) The layer-structure morphology is observed in the MA process and results in the solid-state amorphizing reaction which occurs at the Al/Ta interfaces. In MD, however, there is no layer-structure morphology because the starting material is an intermetallic compound itself.

(3) In the early and intermediate stages of MA, heating the alloy powders to 700 K leads to the formation of an amorphous phase by solid-state diffusion.

(4) The amorphization process by MD is fast and much more homogeneous than by MA.

(5) The amorphous $Al_{50}Ta_{50}$ alloy powders obtained by MA crystallize through a single sharp peak, whereas in MD two broad crystallization peaks are obtained. This may be attributed to nucleation and growth morphology of the MD AlTa alloy powders.

(6) The MD process leads to a rather high iron contamination content in the milled powders. This may be attributed to the relatively high hardness of the AlTa crystalline compound.

Acknowledgments

The authors wish to express their deep thanks to Dr. Y. Minonishi for discussions motivating this investigation. Also, we are grateful to Mr. K. Wakoh and Ms. S. Morita for their technical assistance. We would like to thank the NEC company for providing us with the high-grade tantalum powders and plates used in this study. We are indebted to Mr. Y. Danzaki and Dr. K. Takada for the suggested chemical analysis explanations. Also, many thanks to Mr. F. Wagatsuma for his great support during the EPMA measurements. This work was supported by Ministry of Education, Science and Culture, Grant-in-Aid for Development Scientific Research (B)03555139.

References

1 R. B. Schwarz and W. L. Johnson, *Phys. Rev. Lett.*, *51* (1983) 415.
2 C. C. Koch, O. B. Cavin, C. G. McKamey and J. O. Scarbourgh, *Appl. Phys. Lett.*, *43* (193) 1017.
3 M. Sherif El-Eskandarany, F. Itoh, K. Aoki and K. Suzuki, *J. Non-Cryst. Solids*, *117/118* (1990) 729.
4 M. Sherif El-Eskandarany, K. Aoki and K. Suzuki, in P. H. Shingu (ed.), *Proc. Int. Symp. on Mechanical Alloying (ISMA), Kyoto, Japan, May 7–10, 1991*, in press.
5 M. Sherif El-Eskandarany, K. Aoki and K. Suzuki, *Scripta Metall.*, *25* (1991) 1695.
6 M. Sherif El-Eskandarany, K. Sumiyama, K. Aoki and K. Suzuki, in P. H. Shingu (ed.), *Proc. Int. Symp. on Mechanical Alloying (ISMA), Kyoto, Japan, May 7–10, 1991*, in press.
7 M. Sherif El-Eskandarany, K. Aoki and K. Suzuki, *J. Less-Common Met.*, *166* (1990) 113.
8 A. E. Ermakov, E. E. Yurchikov and V. A. Barinov, *Phys. Met. Metall.*, *52* (1981) 50.
9 J. S. C. Jang and C. C. Koch, *J. Mater. Res.*, (3) (1990) 498.
10 K. Suzuki, *J. Non-Cryst. Solids*, *117/118* (1990) 1.
11 K. Suzuki, *J. Non-Cryst. Solids*, *112* (1989) 23.
12 P. R. Subramanian, D. B. Miracle and S. Mazdiyasni, *Met. Trans.*, *21* (1990) 539.
13 M. Sherif El-Eskandarany, K. Aoki, H. Itoh and K. Suzuki, *J. Less-Common Met.*, *169* (1991) 235–244.
14 M. Sherif El-Eskandarany, K. Aoki and K. Suzuki, *J. Jpn. Soc. Powder and Powder Metall.*, *38* (1991) 59.